Effect of pseudo-Tsai cluster incorporation on the magnetic structures of *R*-Au-Si (*R* = Tb, Ho) quasicrystal approximants

Girma Hailu Gebresenbut,[1] Takayuki Shiino,[2] Mikael Svante Andersson,[1] Navid Qureshi,[3] Oscar Fabelo ©,[3] Premysl Beran ©,[4]
Daniel Qvarngård,[5] Patrik Henelius,[5,6] Andreas Rydh ©,[7] Roland Mathieu,[2] Per Nordblad,[2] and Cesar Pay Gomez ©[1,*]

[1]*Department of Chemistry–Ångström Laboratory, Uppsala University, Box 538, 751 21, Uppsala, Sweden*
[2]*Department of Materials Science and Engineering, Uppsala University, Box 35, 751 03 Uppsala, Sweden*
[3]*Institut Laue-Langevin, 71 avenue des Martyrs, CS 20156, 38042 Grenoble, France*
[4]*European Spallation Source ESS ERIC, Box 176, 221 00 Lund, Sweden*
and Nuclear Physics Institute CAS, Hlavni 160, Řež, 250 68 Husinec, Czech Republic
[5]*Physics Department, KTH Royal Institute of Technology, Roslagstullsbacken 21, 114 21 Stockholm, Sweden*
[6]*Faculty of Science and Engineering, Åbo Akademi University, 20500 Åbo, Finland*
[7]*Department of Physics, Stockholm University, SE-106-91 Stockholm, Sweden*

In cluster-based quasicrystals, tetrahedra located in conventional Tsai clusters may be replaced by single rare-earth (*R*) ions at the cluster centers (pseudo-Tsai clusters). In this study, we investigate the effect of the pseudo-Tsai cluster incorporation on the magnetic structures of two approximants, the Tsai-type Tb-Au-Si [denoted TAS(0)] and Ho-Au-Si [denoted HAS(52)] with partial replacement of conventional Tsai clusters by pseudo-Tsai clusters, up to 52%. The mixture of Tsai and pseudo-Tsai clusters can be considered a different source of randomness/disorder other than the conventional chemical mix sites (Au/Si). The effect of the latter has been previously discussed regarding the origin/cause of spin-glass-like ordering and Anderson localization of electronic states in quasicrystals and approximant crystals. Single crystal neutron diffraction experiments at 2 K were performed and bulk physical properties (magnetization and specific heat) were investigated. In addition, earlier collected powder neutron diffraction data of TAS(14) with 14% replacement was reanalyzed in light of the results on TAS(0) and HAS(52). We find that the arrangement of ordered magnetic spins in the icosahedral shells of these phases is similar, while the cluster-center *R* magnetic states are different. In the case of TAS(14), the cluster-center Tb magnetic moments seem to affect the arrangement of surrounding icosahedral magnetic moments, and the magnetic structure of the icosahedral shell deviates from that of TAS(0). In the case of HAS(52), however, the icosahedral *R* magnetic moments are less affected by the cluster-center *R*, while the averaged cluster-center *R* magnetic moments are significantly diminished. We discuss these results considering the magnetic ordering effect on the bulk physical properties.

I. INTRODUCTION

Since the discovery of the first quasicrystal (QC) [1], several fundamental questions concerning our perception of long-range order and crystallinity itself have puzzled the scientific community. The first is how atoms can be arranged in three dimensions to uphold long-range order (resulting in sharp diffraction peaks) while eluding periodicity [2]. In this regard, unique insights into the atomic order of icosahedral quasicrystals (i-QCs) were revealed with the complete structure determination of the Tsai-type i-YbCd$_{5.7}$ quasicrystal

in 2007 [3]. The second fundamental question concerns the effects of aperiodic order on electronic structure, electrical and magnetic properties, and localization effects [4–6]. With the recent exception of two metastable phases obtained by fast quenching in the *R*-Au-Ga (*R* = Gd, Tb) systems [7], long-range magnetic order has not been observed in stable quasicrystals, although theoretical work has concluded that long-range magnetic order should be possible to realize in a quasiperiodic lattice [8].

The magnetism of i-QCs and their structurally related approximant crystals (ACs) have been well studied. Spin-glass-like behavior has been observed in most of the magnetic i-QCs and ACs, while long-range magnetic ordering has been observed in some ACs: e.g., TbCd$_6$ [9], and several Au-based materials, e.g., *R*-Au-SM (*R* = Gd, Tb, Dy, and Ho; SM = Si, Ge, Sn, Al and Ga) [10–17]. There are several remarkable discoveries: for example, unusual quantum critical phenomena in the Au-Al-Yb i-QC [18] and its AC [19], peculiar short-range magnetic correlations in the Zn-Mg-*R* i-QC [20], and unique noncoplanar and noncollinear

magnetic order in the Tb-Au-Al [21] and Tb-Au-Si ACs [22].

Recently, an interesting type of cluster structure (pseudo-Tsai cluster), which differs from the conventional Tsai-type cluster, was found in a series of R-Au-Si (R = Gd, Tb, and Ho) approximants [17]; the complete replacement of the cluster-center tetrahedra (existing in the Tsai clusters) by single moment bearing R atoms and the successful synthesis of millimeter-sized single crystals indicate that these are equilibrium phases of quasicrystal approximants. This replacement of the cluster-center tetrahedra enables the realization of perfect local icosahedral symmetry since the tetrahedral unit is the only unit breaking the local icosahedral symmetry in Tsai clusters. Note that the tetrahedra in Tsai clusters are generally disordered, and this disorder is what upholds the global high symmetry (cubic or icosahedral) in conventional Tsai-type phases, although locally, this high symmetry is always broken by the presence of tetrahedra. In addition, it has been demonstrated that the partial replacement of Tsai clusters by pseudo-Tsai clusters is also possible [13]. From magnetic property measurements, we found that the magnetic ordering temperatures for Tb-Au-Si approximants decrease as the concentration of pseudo-Tsai clusters increases. Some qualitative changes in the magnetic ordering were also observed between the Tsai and pseudo-Tsai phases; for example, in $Tb_{13.6}Au_{68.6}Si_{17.8}$, referred to as TAS(0), the absence of pseudo-Tsai clusters leads to ferrimagneticlike magnetic ordering while $Tb_{15.3}Au_{67.1}Si_{17.6}$, referred to as TAS(100) and composed only of pseudo-Tsai clusters, exhibits a glassy feature (yet a long-range magnetic ordering seems to be preserved). For this reason, the intermediate compounds TAS(14) and HAS(52) were investigated more closely to ascertain the effect of partial replacement of Tsai clusters by pseudo-Tsai clusters on the magnetic structure. Note that we use similar notations for the R-Au-Si materials throughout this paper; i.e., TAS and HAS refer to the Tb-Au-Si AC and Ho-Au-Si AC, respectively, and the number in the parentheses indicates the percentage of pseudo-Tsai clusters in the structure (note that "IT/CC" was used instead for the 0/100 end compounds in Ref. [17]). However, the effect of pseudo-Tsai clusters on the magnetic state/structure remains to be clarified.

In this study, we have performed single crystal neutron diffraction experiments at 2 K on HAS(52) and TAS(0) to investigate the effect of the pseudo-Tsai clusters on the magnetic state and structures of the systems. We found that the arrangement of magnetic spins in the icosahedral shells of both compounds shows similarities, both exhibiting noncollinear and noncoplanar spin texture with a spiral-like order around the [111] axis. For the conventional Tsai-type approximant TAS(0), we compare the present neutron-scattering experiment result measured at 2 K with a previously reported result measured at 5 K by another group [22]. Bulk magnetic measurements suggest that even such a minor temperature difference may have an effect on the magnetic structure due to the proximity to the magnetic ordering temperature. Furthermore, we investigate the bulk physical properties (magnetization and specific heat), including those of the other end compounds [i.e., HAS(0), HAS(100), and TAS(100)] to elucidate the effect of pseudo-Tsai clusters on the bulk magnetic properties. Note that the magnetization data of the end

compounds [i.e., TAS(0), TAS(100), HAS(0), and HAS(100)] are replotted from Ref. [17], while the specific heat data were collected and investigated in this study. The magnetic ordering is characterized by ferrimagneticlike magnetization behavior [giving the estimated ordering temperature of 3 K for HAS(52) and 10.5 K for TAS(0)] and the broad-peak behavior of the specific heat. In order to investigate the difference between HAS and TAS with respect to the effect of the pseudo-Tsai cluster, we reanalyzed the magnetic structure of TAS(14) using the previously reported neutron powder diffraction data and concluded that the magnetic structure is noncollinear and noncoplanar, similar to that of TAS(0). However, we found that the presence of pseudo-Tsai clusters affect the magnetic structures of HAS(52) and TAS(14) in different ways. The icosahedral magnetic moments in TAS(14) are significantly agitated by the presence of cluster-center Tb magnetic moments. On the other hand, the icosahedral magnetic moments in HAS(52) are less influenced by the cluster-center Ho moment. Instead, the central moment displays a severely diminished moment size.

II. EXPERIMENT

A. Synthesis and characterization

The target compounds, HAS(52) and TAS(0), were prepared by the self-flux synthesis method. Elemental granules of Au (99.99%), Ho (99.9%), and Tb (99.9%) from ChemPUR and Si (99.999%) from Highways International were commercially obtained. A similar synthesis approach as was previously reported (see Ref. [17]) was adapted for the current compounds and further synthesis details are provided in the Supplemental Material [23], which includes Ref. [24]. The synthesis of the TAS(14) sample used for comparison was described earlier in Ref. [12].

A Bruker D8 powder diffractometer with Cu radiation ($K\alpha_1 = 1.5406$ Å and $K\alpha_2 = 1.54443$ Å) was used to collect powder x-ray diffraction (PXRD) patterns from polycrystalline samples at room temperature. PXRD profile fitting was done using the FULLPROF SUITE software [25]. A Bruker D8 single crystal x-ray diffractometer with Mo radiation ($K\alpha = 0.71073$ Å) coupled with an Incoatec Microfocus Source (IμS) (beam size ≈ 100 μm at the sample position) and an APEXII CCD area detector (6 × 6 cm) was utilized to collect single crystal x-ray diffraction (SCXRD) intensities. Data reduction and numerical absorption corrections were performed using the Bruker APEXII software [26]. The JANA2006 software package [27] was used for atomic structure determination from SCXRD data which utilizes the charge flipping method for structure solution prior to refinement. Single crystal neutron diffraction (SCND) measurements were performed at the ILL facility on the D9 and D10 beamlines using a four-cycle diffractometer with neutron wavelengths of 0.8403 and 2.36 Å, respectively. The crystals were first checked with the help of a Laue neutron diffraction camera at Orient Express (ILL). Nuclear and magnetic Bragg reflections were measured at temperatures of 2 and 20 K. The FULLPROF SUITE software package, which utilizes simulated annealing and Rietveld refinement methods, was applied to initially determine and refine nuclear and magnetic structures from SCND data. A
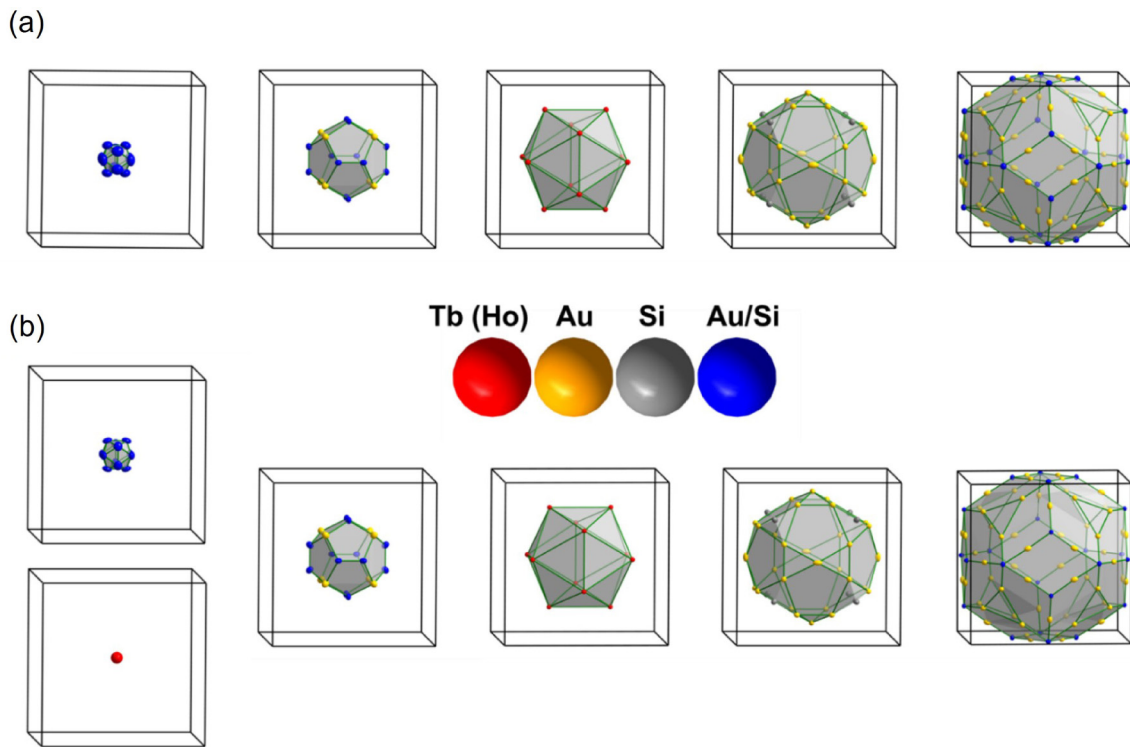
FIG. 1. Concentric polyhedral shells of the Tsai-type cluster unit in (a) TAS(0) and (b) HAS(52). Arranged from the left (inside) to the right (outside) are a disordered tetrahedron [and Ho atom in (b)], pentagonal dodecahedron, icosahedron, icosidodecahedron, and defect rhombic triacontahedron. For simplicity, only one cluster unit is shown at the center of the unit cell but it should be noted that identical clusters are also present at the vertices. All atomic sites are represented by thermal ellipsoids at the 50% probability level. The sizes of the polyhedra are scaled with respect to the unit cell size.

Zeiss 1550 scanning electron microscope (SEM) instrument coupled with an energy dispersive x-ray detector (EDX) was employed for elemental analyses. The dc magnetization was recorded as a function of temperature in the magnetic field $H = 10$ Oe using a superconducting quantum interference device (SQUID) magnetometer from Quantum Design Inc. The dc magnetization was recorded as a function of magnetic field up to ± 50 kOe at $T = 2$ K on the same instrument. The specific heat data were collected using a differential membrane-based nanocalorimeter [28] down to ~ 100 mK in magnetic fields up to 120 kOe. For the magnetization and heat capacity measurements, we used polycrystalline materials.

B. Structure refinements

The atomic structures of the HAS(52) and TAS(0) were determined from SCXRD data prior to the SCND experiment. The SCXRD refinement results are presented in Table S1 and Fig. S2 in the Supplemental Material [23]. The atomic structures of both compounds are similar to previous reports in similar R-Au-SM [10,12,17]. Hence, to avoid redundancy, a short summary is presented here. However, it should be noted that the structure refinement result for the HAS(52) compound has never been previously reported. As shown in Fig. 1, Tsai clusters are located at the corner and body center of a cubic unit cell. The basic Tsai cluster is made of five concentric polyhedra shells. The subsequent atomic shells from the cluster center and out are a disordered tetrahedron, a dodecahedron, an icosahedron, an icosidodecahedron, and

a defect rhombic triacontahedron. The disordered tetrahedron in the Ho-Au-Si AC was partially replaced by a single Ho site (52 at. % occupancy) located at the cluster center, the so-called central Ho. This is the peculiar structural feature that often appears in Au-containing ternary Tsai-type 1/1 ACs. The mutually exclusive behavior between the disordered tetrahedron and the central-R position, and the effects on magnetic properties are further discussed in [13,17]. In the compound TAS(0), there is no heavy central-Tb atom, but only the disordered tetrahedron is present at the cluster center.

The large single crystals grown for TAS(0) and HAS(52) were used to collect SCND data at the D10 and D9 beamlines, respectively, on the reactor-based neutron source at the ILL. For the Ho sample in particular, a large number of nuclear and magnetic intensities could be collected in order to study both the nuclear and magnetic structures in detail. Two datasets were collected for each sample: one above the magnetic transition temperature T_N and the other below. No additional magnetic peaks were detected below T_N for any of the samples, but a clear increase of the diffraction intensities at the nuclear Bragg positions was detected, confirming the ferro- or ferrimagnetic nature of the samples with propagation vector $\boldsymbol{k} = 0$. Initial refinement of the magnetic structure was attempted on a dataset containing only the magnetic contributions to the Bragg intensities, which were extracted by subtracting the integrated intensities collected above the magnetic transition temperatures T_N, from those collected below. At first, refinements were performed in every possible magnetic space group related to the parent space group $Im\bar{3}$
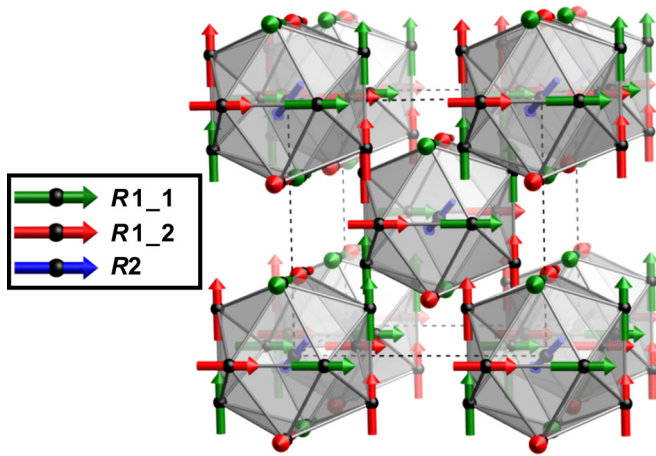
FIG. 2. Ideal magnetic structure of ferromagnetic (ferrimagnet-iclike) R-Au-Si 1/1 ACs (R = Tb, Ho). Independent magnetic moments are colored in red, green, and blue, and named according to their associated R sites.

of the paramagnetic nuclear structure. The best refinement was obtained in the rhombohedral magnetic space group $R\bar{3}$ (No. 148.1.1247 in OG notation and 148.17 in BNS notation) [29,30], taking into account R values vs the number of parameters.

Independently, an attempt was made to solve the magnetic structure by simulated annealing removing all symmetry restrictions except the body-centering translation. In this latter case, the simulation converged into a structure solution that clearly had a true symmetry higher than $P1$. The obtained model was tested for higher symmetry using the program PSEUDOSYMMETRY SEARCH [31] on the Bilbao Crystallo-
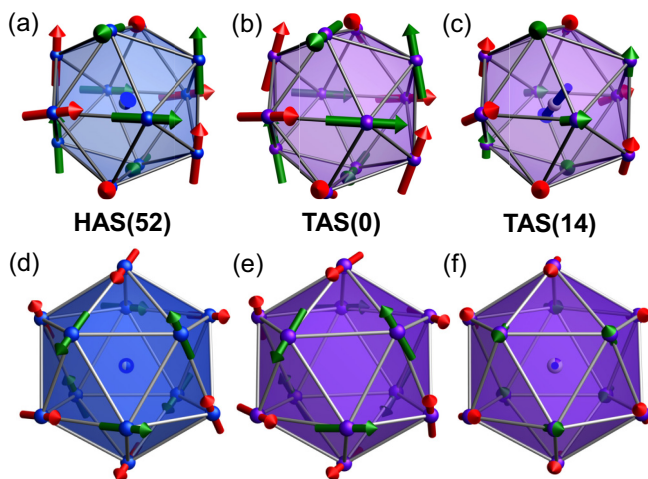
graphic Server, and the symmetry analysis revealed that the true symmetry of the magnetic structure once again was $R\bar{3}$. In other words, the same magnetic space group symmetry was obtained by two independent routes, reassuring its validity.

The basic magnetic structures of the Tb and Ho compounds were found to be similar, and the refined structures agree with a model presented by Hiroto *et al.* [22] for the Tb compound. The single crystal data further improve upon a previously reported model based solely on powder neutron diffraction data, which assumed the simplest collinear arrangement of magnetic spins [12]. Furthermore, the herein proposed model solved the problem of largely unequal moments on the equivalent R positions in the nuclear structure and the magnetic moments now agree well with those expected for the corresponding R elements Tb and Ho, as seen in Figs. 2 and 3 and Table I. Based on this result, the previously collected powder neutron data on a Tb-Au-Si sample with 14% Tb occupancy at the cluster center [herein denoted TAS(14)] [12], was revisited and fitted to the newly obtained rhombohedral model. The agreement to these powder data previously collected at ISIS was excellent and the results of the fit are presented in Fig. S3 in the Supplemental Material [23]. Note that the refinement was performed against data collected on all five detector banks simultaneously. In all magnetic structure refinements (powder and single crystal alike), the rhombohedral symmetry was applied to the magnetic structure in a nonstandard setting: the cubic metrics ($a = b = c$ and $\alpha = \beta = \gamma = 90°$) and body centering were kept throughout the refinement effectively resulting in an $I\bar{3}$ magnetic space group. The cubic $Im\bar{3}$ symmetry was, however, enforced on the nuclear structure through equations affecting only the nuclear part of the structure in the program JANA2006. These equations were formulated to reproduce all the symmetry operations lost in the transition from the space group $Im\bar{3}$ to $I\bar{3}$. Imposing cubic symmetry only on the nuclear structure resulted in a much more stable refinement and drastically reduced the number of parameters providing a high degree of overdetermination. The action is further justified by the fact that no indication of deviations from cubic symmetry in the nuclear structures was observed in any of the diffraction or other experimental data collected for the R-Au-Si (R = Ho and Tb) approximants.

The number of symmetry operations lost in going from the cubic space group $Im\bar{3}$ to rhombohedral $I\bar{3}$ also determines the number of resulting magnetic domains and their relative orientations. Based on these symmetry considerations, we conclude that eight independent magnetic domains form; however, those related by the time-reversal operation will contribute coherently to the same reflections and are

FIG. 3. Refined magnetic moments and their arrangements on the atomic clusters of the investigated R-Au-Si 1/1 ACs. All magnetic moments are drawn on a common scale for easy comparison. (a–c) are plotted for the comparison with Fig. 2, while (d–f) are views from the [111] direction. The refined numerical values of the moments are shown in Table I.

TABLE I. Refined magnetic moments of HAS(52), TAS(0), and TAS(14).

R compound	Position		
	$R1\_1$	$R1\_2$	$R2$
HAS(52)	7.71(7) μ_B	7.74(2) μ_B	0.85(42) μ_B
TAS(0)	8.53(2) μ_B	9.02(2) μ_B	–
TAS(14)	3.56(92) μ_B	5.59(22) μ_B	8.66(58) μ_B

thus indistinguishable. Thus, the number of refinable domain volumes with rhombohedral symmetry amounts to four, and their relative orientations are defined by the following four symmetry operators:

$$\begin{bmatrix} h' \\ k' \\ l' \end{bmatrix} = \begin{bmatrix} 1 & 0 & 0 \\ 0 & 1 & 0 \\ 0 & 0 & 1 \end{bmatrix} \times \begin{bmatrix} h \\ k \\ l \end{bmatrix},$$

$$\begin{bmatrix} h' \\ k' \\ l' \end{bmatrix} = \begin{bmatrix} -1 & 0 & 0 \\ 0 & -1 & 0 \\ 0 & 0 & 1 \end{bmatrix} \times \begin{bmatrix} h \\ k \\ l \end{bmatrix},$$

$$\begin{bmatrix} h' \\ k' \\ l' \end{bmatrix} = \begin{bmatrix} 1 & 0 & 0 \\ 0 & -1 & 0 \\ 0 & 0 & 1 \end{bmatrix} \times \begin{bmatrix} h \\ k \\ l \end{bmatrix},$$

$$\begin{bmatrix} h' \\ k' \\ l' \end{bmatrix} = \begin{bmatrix} 0 & 1 & 0 \\ 0 & 0 & -1 \\ -1 & 0 & 0 \end{bmatrix} \times \begin{bmatrix} h \\ k \\ l \end{bmatrix}.$$

The refined domain volumes, crystallographic data, and F_{obs} vs F_{calc} plots for the magnetic structure refinements of the HAS(52) and TAS(0) single crystal samples with different R occupancies at the cluster centers (given in parentheses) are presented in Table S3 and Fig. S4 in the Supplemental Material [23].

The HAS(52) and TAS(0) structures were refined from single crystal neutron diffraction data. The initial refinements were performed against only the extracted magnetic contributions to the diffraction intensities. The resulting magnetic structures were, in essence, similar to the final refined structures; however, at this stage, some of the magnetic domain volumes were refined to unrealistically low values and the refined magnetic moments were significantly lower than the theoretical values. The final refinement was, therefore, carefully performed against single datasets collected at 1.8 K. The magnetic intensities were not treated separately; instead, the nuclear and magnetic structures were refined simultaneously while imposing cubic constraints on the atomic positions, locking the atomic displacement parameters and relaxing the magnetic structure under rhombohedral constraints. This procedure did neither infer large changes to the nuclear nor the magnetic structures, but the small changes were sufficient to obtain lower R values, physically sound domain volumes, and magnetic moments for the R atoms.

III. RESULTS AND DISCUSSION

A. Single crystal neutron diffraction

In Figs. 3(a)–3(f), we see the distribution of refined magnetic moments in Tb-Au-Si and Ho-Au-Si approximants. Note that Figs. 3(a)–3(c) are shown to compare with the ideal model seen in Fig. 2, while Figs. 3(d)–3(f) show views along the [111] direction in which the spiral-like spin arrangement around the [111] axis is visible. Green ($R1\_1$) and red ($R1\_2$) sublattices are the two types of independent moments in the icosahedral shell (as in Fig. 2). The blue ($R2$) moments correspond to the partially occupied R sublattice at the cluster center. The refined sizes of the magnetic moments and their uncertainties are listed in Table I. It is clearly seen that the magnetic moments of the TAS(14) approximant are signif-

icantly quenched on the icosahedral shell as compared to TAS(0), which has no Tb atom at the cluster center. Note that the reciprocal space in the investigated samples has been thoroughly examined for nonrandom long-range order between tetrahedra and R atoms at the cluster centers, but no superlattice reflections have been observed in our diffraction experiments.

In the TAS(0) compound, the difference in the magnetic moments between the two independent R sites is rather small. The magnitude of the magnetic moments is close to the theoretical value expected for Tb^{3+} ($g_J J \mu_B = 9 \mu_B/Tb^{3+}$). For the Ho compound HAS(52), this difference is even smaller between the sites but the refined values are lower than those expected for, for example, the Ho^{3+} ion ($g_J J \mu_B = 10 \mu_B/Ho^{3+}$), which may be attributed to the measurement temperature as discussed below. The main difference between the Ho- and Tb-containing approximants is a slight angular tilt of the icosahedral moments, where the Ho compound is closer to the ideal structure in Fig. 2 with moments aligning along the axial directions of the nuclear cubic unit cell, as seen by comparing Figs. 3(a) and 3(b). The Tb compounds, on the other hand, show a slight tilt of the moments with a tendency to be perpendicular to the fivefold directions of the icosahedral R clusters (cf. Fig. 3) [21,22]. Another difference between the Ho and Tb compounds is seen in the R atoms at the cluster center. If we compare HAS(52) with TAS(14), which both have nonzero occupancy at the cluster center, we see that the refined magnetic moment at this position for the Ho compound is close to zero, while the largest moment in the whole structure is found here in the case of the Tb compound. Both the neutron data and single crystal x-ray data resulted in good refinements for the nuclear structure with clearly observable scattering densities at the 0 0 0 position, which was refined to close to 50% occupancy of Ho for x-ray and neutron single crystal data, respectively, indicating that this occupancy is indeed reliable and can be attributed solely to Ho. The high occupancy of Ho at the cluster center should certainly be enough to make a clear contribution to the magnetic Bragg intensities, and trials with different oxidation states for this Ho atom still gave the same result.

From the refinement of the neutron-scattering data, we obtain the value of averaged icosahedral magnetic moments at 2 K: $8.5 - 9.0 \mu_B/Tb$ for TAS(0), $3.5 - 5.6 \mu_B/Tb$ for TAS(14), and $7.7 \mu_B/Ho$ for HAS(52). In the case of TAS(14), the present result indicates that the cluster-center Tb ions affect the magnetic state (orientation) of the surrounding icosahedral R magnetic moments, as seen in Fig. 3. This indicates that there should be a significant magnetic interaction between a cluster-center R magnetic moment and the surrounding 12 icosahedral R magnetic moments. In the case of HAS(52), however, the effect of cluster-center Ho on the icosahedral Ho ions seems to be less significant, as indicated by our observation that the orientation of icosahedral magnetic moments of HAS(52) is similar to that of the Tsai-type one [i.e., TAS(0)].

B. Magnetization

The inverse susceptibility of the $4f$ electron contribution was found to depend linearly on temperature (i.e., Curie-
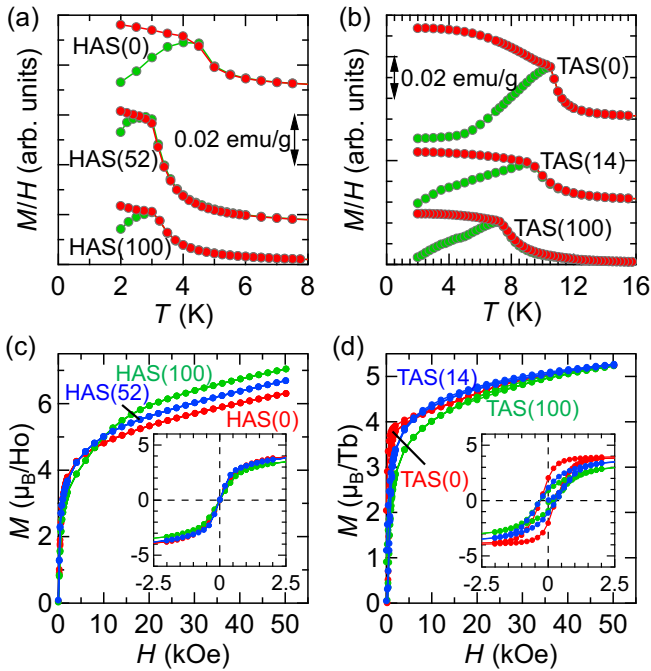
FIG. 4. (a,b) Temperature dependence of the ZFC (green) and FC (red) magnetization *M* (plotted as *M/H*) recorded in an applied magnetic field $H = 10$ Oe for (a) the HAS compounds [HAS(0), HAS(52), HAS(100)] and (b) the TAS compounds [TAS(0), TAS(14), and TAS(100)]. Note that the *M/H*(*T*) curves have been arbitrarily shifted from the origin. (c,d) Magnetic-field dependence of the magnetization of (c) the HAS compounds and (d) the TAS compounds recorded at $T = 2$ K. The insets show close-up views of the low-field region. Note that the data presented here for HAS(0), HAS(100), TAS(0), and TAS(100) are from Ref. [17]. The magnetization for TAS(14) studied in Ref. [12] was remeasured.

Weiss behavior) in a wide temperature range from room temperature to low temperature: see the Supplemental Material [23] for HAS(52); Ref. [17] for the end compounds HAS(0), HAS(100), TAS(0), and TAS(100); and Ref. [12] for TAS(14). The extracted effective magnetic moment (at high temperatures) values were 10.85, 11.02, 9.86, 9.84, and $10.2\,\mu_B/R$ ($R =$ Tb, Ho), respectively. In the case of HAS(52), the extracted Curie-Weiss temperature was 2.9 K, and the effective magnetic moment was $10.8\,\mu_B/$Ho (see Supplemental Material). All these values are in good agreement with the theoretical value expected for the free R^{3+} ions ($9.72\,\mu_B/$Tb^{3+}, $10.6\,\mu_B/$Ho^{3+}). This indicates that $4f$ electrons are well localized in these systems. The estimated Curie-Weiss temperature is positive for these systems indicating that ferromagnetic interaction is dominant.

Figures 4(a) and 4(b) show the dc magnetization of the HAS and the TAS compounds. Note that the magnetization data (including *M-H* curves) for HAS(0), HAS(100), TAS(0), and TAS(100) are from Ref. [17]. The HAS compounds and TAS(0) exhibit ferrimagnetic transition, while TAS(14) and TAS(100) exhibit somehow similar magnetization curves, with a broader onset of magnetic ordering. From the zero-field cooled (ZFC) and field cooled (FC) magnetization curves, we estimate the magnetic ordering temperatures to be 3 K

for HAS(52), 9 K for TAS(14), and 10.5 K for TAS(0). As seen in Figs. 4(c) and 4(d), the *M-H* curves (at $T = 2$ K) of both materials are ferrimagneticlike with no saturation up to 50 kOe. The magnetization at $H = 50$ kOe amounts to $\sim 5.5\,\mu_B/$Tb for the TAS compounds and $6 - 7\,\mu_B/$Ho for the HAS compounds. These values are smaller than the theoretical values of $g_J J\mu_B = 9\,\mu_B/$Tb and $10\,\mu_B/$Ho (calculated considering Tb^{3+} and Ho^{3+}, as suggested by the results of the Curie-Weiss analyses), which is most probably due to a crystal electric field (CEF) effect. We observe hysteresis behavior for the TAS compounds (with a coercivity of $\sim$300 Oe) while there is no clear hysteresis in the HAS compounds. Note that the measurement temperature 2 K is just below the transition temperature ($\sim$3 K).

C. Specific heat

Figure 5 shows the temperature dependence of the specific heat divided by temperature (*C/T*) for the HAS and TAS compounds except for TAS(14). We observe a significant increase in *C/T* below $\sim$1 K for both HAS and TAS systems, which is attributed to the Ho and Tb nuclear contributions (C_{nuc}), respectively [32,33]; see the Supplemental Material [23]. We do not observe a significant difference in C_{nuc} depending on applied magnetic fields. This must be due to huge internal effective magnetic fields (compared to the applied external magnetic fields) on the Ho and Tb nuclei [32,33]. To estimate the contributions from the magnetic transitions, we calculate $C_{mag} = C_{H=0} - C_{H=100/120\,kOe}$, in which the electronic, phonon, and nuclear contributions cancel out. Note that $C_{H=0}$ is the zero-field specific heat, while $C_{H=100/120\,kOe}$ is the specific heat under the magnetic field of $H = 100$ [for HAS(0) and HAS(100)] or 120 kOe [for HAS(52), TAS(0) and TAS(100)], in which the magnetic ordering is suppressed significantly (see Fig. 5). Figures 6(a) and 6(b) show the temperature dependence of C_{mag}/T for the HAS and TAS compounds. We observe clear broad peaks in C_{mag}/T corresponding to the magnetic transitions. These peaks are suppressed by the application of external magnetic fields (see Fig. 5). We calculate the magnetic entropy using the following equation,

$$\Delta S_{mag}(T) \equiv \int_{T_{base}}^{T} \frac{C_{mag}(T')}{T'} dT',$$

where T_{base} ($\sim$0.5 K) is the base temperature of the analysis, and ΔS_{mag} means the magnetic entropy measured from $T_{base} \sim 0.5$ K. Figures 6(c) and 6(d) show the temperature dependence of the magnetic entropy (ΔS_{mag}) for the HAS and TAS compounds. For the present HAS and TAS systems, ΔS_{mag} gains nearly Rln(2) (where R is the gas constant) around the magnetic ordering temperature T_{mag}, suggesting that their CEF ground states are doublet. Note that the slight deviations from the Rln(2) value should be attributed to the current method of estimation of C_{mag} and/or the missing contribution below $T_{base} \sim 0.5$ K.

D. Discussion

The present study shows microscopically that the effect of pseudo-Tsai clusters on the overall magnetic state signif-
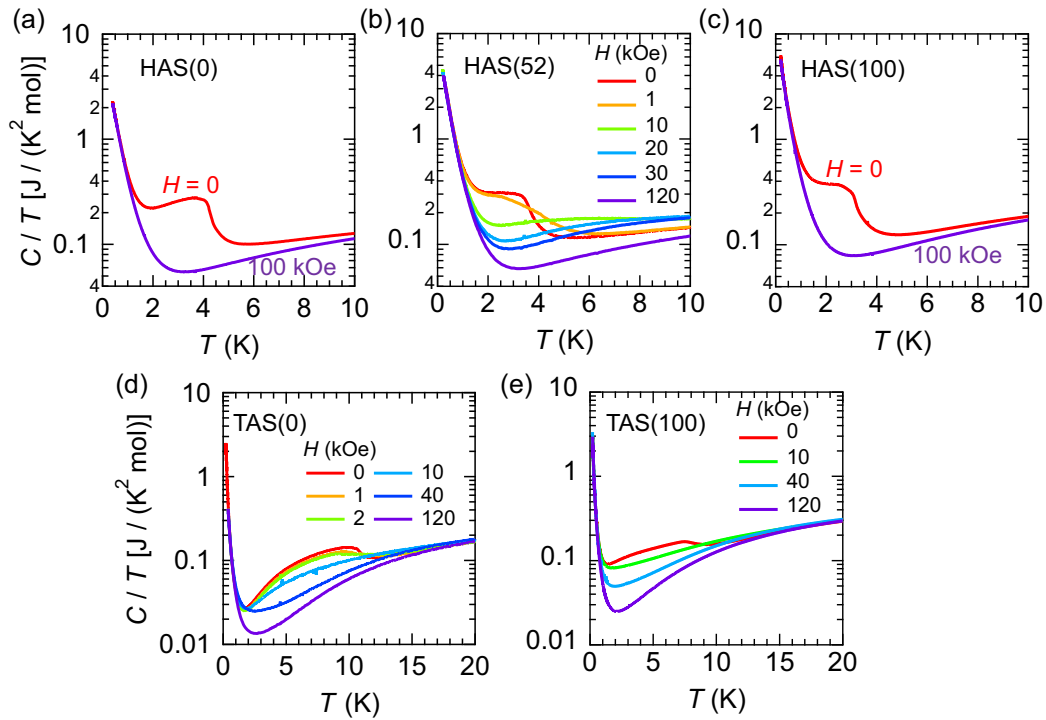
FIG. 5. Temperature dependence of C/T under various values of magnetic fields for (a) HAS(0), (b) HAS(52), (c) HAS(100), (d) TAS(0), and (e) TAS(100). Note that the vertical axes are on a logarithmic scale.

icantly differs depending on R atoms, as summarized and discussed below. First, the magnetic structure of TAS(14) is significantly affected by the cluster-center Tb ions, as shown

FIG. 6. (a,b) Temperature dependence of C_{mag}/T for (a) the HAS compounds and (b) the TAS compounds. (c,d) Temperature dependence of the magnetic entropy estimated from the C_{mag}/T data for (c) the HAS compounds and (d) the TAS compounds. See the main text for the definition of C_{mag} and ΔS_{mag}.

in Fig. 3; the angular tilts of the icosahedral Tb moments in TAS(14) have slightly shifted as compared to TAS(0), and clearly show much diminished magnetic moments. We speculate that the cluster-center magnetic moments give additional frustration and randomness [through the Ruderman-Kittel-Kasuya-Yosida (RKKY) magnetic interaction] [34] between the cluster-center moments and the surrounding icosahedral moments. The magnetic moment of cluster-center Tb in TAS(14) shows a nearly full Tb moment (8.66 μ_B, which is close to $g_J J \mu_B = 9$ μ_B for Tb^{3+}) in contrast to the surrounding Tb ions on the icosahedral shell. This infers that the icosahedral Tb moments tend to be magnetically frustrated more than the central ones in the present TAS(14) system. The presence of 14% pseudo-Tsai clusters in TAS(14) may disturb the long-range magnetic order due to the spatial disorder and thus cause a decrease in the average moment size of icosahedral Tb moments. Our finding indicates that even the partial existence of pseudo-Tsai clusters changes the magnetic state/structures significantly.

In the case of HAS(52), the average central Ho moment is significantly quenched to near zero, while the icosahedral moments seem to be less influenced. This behavior is contrasted with that of TAS(14). A possible compounding contribution to the low magnitude of the cluster-center magnetic moment is the high symmetry of the site. The local field on a given center site generated by its nearest neighbors could be relatively small due to canceling contributions to the field components, leading to larger amplitudes in thermal moment direction fluctuations. These fluctuations, in turn, would make the average of the central site moments seem smaller in magnitude due to the induced spatial disorder. This possibility is supported
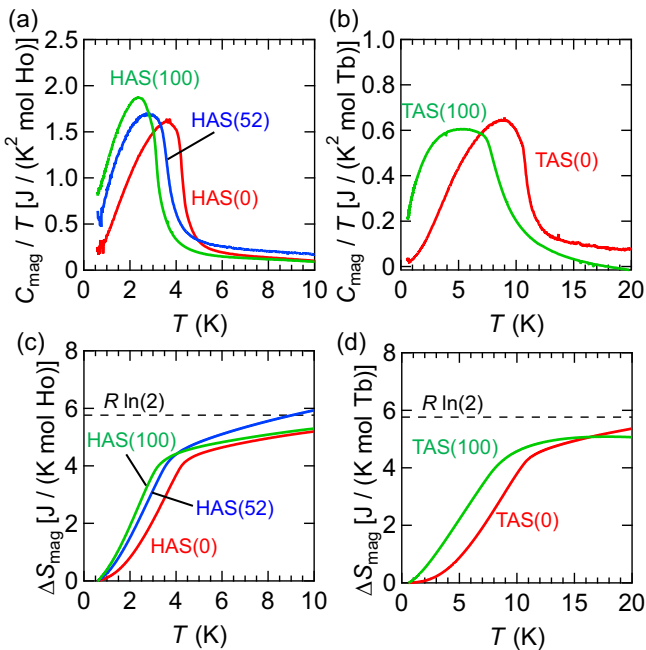
by Monte Carlo simulations presented in the Supplemental Material [23] and considering the following discussion.

The somewhat diminished size of the icosahedral Ho moment in HAS(52) (compared, for example, to $g_J J \mu_B = 10 \; \mu_B$ for Ho^{3+}) may be attributed to the incomplete alignment of magnetic moments at the measurement temperature 2 K, which is very close to the ordering temperature ∼3 K. Note that the spatial fluctuation of CEF might also partly contribute to diminishing the moment size as discussed in Ref. [22]. The specific heat of these systems exhibits a broad peak below the transition temperature [see Figs. 6(a) and 6(b)]. Furthermore, by studying the time-dependent dc magnetization and ac magnetic susceptibility of the compounds, we have observed glassy features of the TAS compounds right below the transition temperature [35]. These findings suggest that some magnetic frustration exists in these systems. This consideration reasonably explains the difference in the Tb moment size of TAS(0) between the value obtained at 2 K (8.5–9.0 μ_B) in the present study and that at 5 K (6.9 μ_B) from Ref. [22]; i.e., the static magnetic ordering may not be complete at 5 K.

Finally, when comparing the magnetic structures of the herein presented R-Au-Si (R = Ho and Tb) approximants with that of the previously reported antiferromagnetic Tb-Au-Al approximant [21], we find that the ordering of spins at the cluster level has similarities, forming a spiral-like arrangement in the icosahedral shell [see Figs. 3(d)–3(f)]. The main difference between the magnetic structures of the R-Au-Si and Tb-Au-Al Tsai-type approximants is that there is a resulting finite net cluster moment of each cluster along the [111] direction in the R-Au-Si case and the net cluster moments are aligned in parallel, while the net magnetic moment of each cluster is zero in the R-Au-Al case, yet the cluster magnetic-toroidal multipoles are arranged in an antiferroic/alternating way [21]. A curious observation is that these cluster-cluster spin interactions along threefold directions can be associated with the so-called c linkages in Tsai-type approximants and quasicrystals. If the observed spin arrangement at the cluster level is robust not only in the approximants but also in the quasicrystals, it will allow the decoration of b and c linkages with magnetic clusters that interact according to the odd-even parity rules that for atomic icosahedral quasicrystals give rise to P- or F-type icosahedral lattices. Consequently, we can envisage P- and F-type magnetic lattices caused by ferromagnetic and antiferromagnetic cluster-cluster interactions, respectively, decorating the b and c linkages of a magnetic quasicrystal.

IV. CONCLUSION

From the single-crystal neutron diffraction experiments performed at 2 K on HAS(52) and TAS(0), we found that both materials have similar spiral-like magnetic ordering with respect to the icosahedral R moments. The magnetic structure of TAS(14), which was reinvestigated in this study based on previous neutron powder diffraction data [12], also exhibits a magnetic structure in the icosahedral shell similar to that of TAS(0) and HAS(52) but with severely diminished magnetic moments. We have observed microscopically that the effect of pseudo-Tsai cluster incorporation on the overall magnetic state is significant and differs depending on the choice of R atom: TAS(14) exhibits icosahedral moments agitated by the cluster-center moments (which exhibits a nearly full-moment size), while HAS(52) exhibits less influence on the icosahedral moments by the cluster-center moment, which is significantly diminished. Pseudo-Tsai clusters seem to induce randomness/frustration (through the RKKY interaction) in the present systems, yet their unique long-range magnetic order survives.

[1] D. Shechtman, I. Blech, D. Gratias, and J. W. Cahn, Metallic Phase with Long-Range Orientational Order and No Translational Symmetry, Phys. Rev. Lett. **53**, 1951 (1984).

[2] P. Bak, Icosahedral Crystals: Where Are the Atoms? Phys. Rev. Lett. **56**, 861 (1986).

[3] H. Takakura, C. P. Gómez, A. Yamamoto, M. De Boissieu, and A. P. Tsai, Atomic structure of the binary icosahedral Yb-Cd quasicrystal, Nat. Mater. **6**, 58 (2007).

[4] N. K. Sato, T. Ishimasa, K. Deguchi, and K. Imura, Effects of electron correlation and geometrical frustration on magnetism of icosahedral quasicrystals and approximants—an attempt to bridge the gap between quasicrystals and heavy fermions, J. Phys. Soc. Jpn. **91**, 072001 (2022).

[5] S. Sarkar, M. Krajčí, P. Sadhukhan, V. K. Singh, A. Gloskovskii, P. Mandal, V. Fournée, M.-C. de Weerd, J. Ledieu, and I. R. Fisher, Anderson localization of electron states in a quasicrystal, Phys. Rev. B **103**, L241106 (2021).

[6] Y. K. Vekilov, E. I. Isaev, and S. F. Arslanov, Influence of phason flips, magnetic field, and chemical disorder on the localization of electronic states in an icosahedral quasicrystal, Phys. Rev. B **62**, 14040 (2000).

[7] R. Tamura, A. Ishikawa, S. Suzuki, T. Kotajima, Y. Tanaka, T. Seki, N. Shibata, T. Yamada, T. Fujii, and C.-W. Wang, Experimental observation of long-range magnetic order in icosahedral quasicrystals, J. Am. Chem. Soc. **143**, 19938 (2021).

[8] R. Lifshitz, Symmetry of Magnetically Ordered Quasicrystals, Phys. Rev. Lett. **80**, 2717 (1998).

[9] R. Tamura, Y. Muro, T. Hiroto, K. Nishimoto, and T. Takabatake, Long-range magnetic order in the quasicrystalline approximant Cd$_6$Tb, Phys. Rev. B **82**, 220201(R) (2010).

[10] T. Hiroto, G. H. Gebresenbut, C. P. Gómez, Y. Muro, M. Isobe, Y. Ueda, K. Tokiwa, and R. Tamura, Ferromagnetism and re-entrant spin-glass transition in quasicrystal approximants Au-SM-Gd (SM = Si, Ge), J. Phys.: Condens. Matter **25**, 426004 (2013).

[11] T. Hiroto, K. Tokiwa, and R. Tamura, Sign of canted ferromagnetism in the quasicrystal approximants Au-SM-R (SM = Si, Ge and Sn/R = Tb, Dy and Ho), J. Phys.: Condens. Matter **26**, 216004 (2014).

[12] G. Gebresenbut, M. S. Andersson, P. Beran, P. Manuel, P. Nordblad, M. Sahlberg, and C. P. Gomez, Long range ordered magnetic and atomic structures of the quasicrystal approximant in the Tb-Au-Si system, J. Phys.: Condens. Matter **26**, 322202 (2014).

[13] G. H. Gebresenbut, M. S. Andersson, P. Nordblad, M. Sahlberg, and C. Pay Gómez, Tailoring magnetic behavior in the Tb-Au-Si quasicrystal approximant system, Inorg. Chem. **55**, 2001 (2016).

[14] A. Ishikawa, T. Hiroto, K. Tokiwa, T. Fujii, and R. Tamura, Composition-driven spin glass to ferromagnetic transition in the quasicrystal approximant Au-Al-Gd, Phys. Rev. B **93**, 024416 (2016).

[15] A. Ishikawa, T. Fujii, T. Takeuchi, T. Yamada, Y. Matsushita, and R. Tamura, Antiferromagnetic order is possible in ternary quasicrystal approximants, Phys. Rev. B **98**, 220403(R) (2018).

[16] K. Inagaki, S. Suzuki, A. Ishikawa, T. Tsugawa, F. Aya, T. Yamada, K. Tokiwa, T. Takeuchi, and R. Tamura, Ferromagnetic 2/1 quasicrystal approximants, Phys. Rev. B **101**, 180405(R) (2020).

[17] G. Gebresenbut, T. Shiino, D. Eklöf, D. C. Joshi, F. Denoel, R. Mathieu, U. Häussermann, and C. Pay Gómez, Atomic-scale tuning of Tsai-type clusters in Re–Au–si systems (RE = Gd, Tb, Ho), Inorg. Chem. **59**, 9152 (2020).

[18] K. Deguchi, S. Matsukawa, N. K. Sato, T. Hattori, K. Ishida, H. Takakura, and T. Ishimasa, Quantum critical state in a magnetic quasicrystal, Nat. Mater. **11**, 1013 (2012).

[19] S. Matsukawa, K. Deguchi, K. Imura, T. Ishimasa, and N. K. Sato, Pressure-driven quantum criticality and t/H scaling in the icosahedral Au–Al–Yb approximant, J. Phys. Soc. Jpn. **85**, 063706 (2016).

[20] T. J. Sato, H. Takakura, A. P. Tsai, and K. Shibata, Magnetic excitations in the Zn-Mg-Tb icosahedral quasicrystal: An inelastic neutron scattering study, Phys. Rev. B **73**, 054417 (2006).

[21] T. J. Sato, A. Ishikawa, A. Sakurai, M. Hattori, M. Avdeev, and R. Tamura, Whirling spin order in the quasicrystal approximant $Au_{72}Al_{14}Tb_{14}$, Phys. Rev. B **100**, 054417 (2019).

[22] T. Hiroto, T. J. Sato, H. Cao, T. Hawai, T. Yokoo, S. Itoh, and R. Tamura, Noncoplanar ferrimagnetism and local crystalline-electric-field anisotropy in the quasicrystal approximant $Au_{70}Si_{17}Tb_{13}$, J. Phys.: Condens. Matter **32**, 415802 (2020).

[23] See Supplemental Material at http://link.aps.org/supplemental/10.1103/PhysRevB.106.184413 for additional information about sample preparation, structural analysis, neutron diffraction measurements, physical property data, and the Monte Carlo study.

[24] H. Okamoto and T. B. Massalski, The Au−Si (gold-silicon) system, Bull. Alloy Phase Diagrams **4**, 190 (1983).

[25] J. Rodríguez-Carvajal, Recent advances in magnetic structure determination by neutron powder diffraction, Physica B: Condensed Matter **192**, 55 (1993).

[26] APEX 3 software for CCD diffractometers (Bruker Analytical X-ray Systems Inc., Madison, WI, 2014).

[27] V. Petříček, M. Dušek, and L. Palatinus, Crystallographic computing system JANA2006: General features, Z. Kristallogr. - Cryst. Mater. **229**, 345 (2014).

[28] S. Tagliati, V. M. Krasnov, and A. Rydh, Differential membrane-based nanocalorimeter for high-resolution measurements of low-temperature specific heat, Rev. Sci. Instrum. **83**, 055107 (2012).

[29] W. Opechowski and R. Guccione, *Magnetism*, edited by GT Rado and H. Suhl, Vol. 2A (Academic Press, New York, 1965), Chap. 3, p. 105.

[30] N. V. Belov, N. N. Neronova, and T. S. Smirnova, Shubnikov groups, Kristallografiya **2**, 315 (1957).

[31] C. Capillas, E. S. Tasci, G. de la Flor, D. Orobengoa, J. M. Perez-Mato, and M. I. Aroyo, A new computer tool at the Bilbao Crystallographic Server to detect and characterize pseudosymmetry, Z. Kristallogr. - Cryst. Mater. **226**, 186 (2011).

[32] E. C. Heltemes and C. A. Swenson, Nuclear contribution to the heat capacity of terbium metal, J. Chem. Phys. **35**, 1264 (1961).

[33] O. V. Lounasmaa, Specific heat of holmium metal between 0.38 and 4.2 °K, Phys. Rev. **128**, 1136 (1962).

[34] M. A. Ruderman and C. Kittel, Indirect exchange coupling of nuclear magnetic moments by conduction electrons, Phys. Rev. **96**, 99 (1954).

[35] T. Shiino, F. Denoel, G. H. Gebresenbut, C. P. Gómez, P. Nordblad, and R. Mathieu, Nonequilibrium dynamical behavior in noncoplanar magnets with chiral spin texture, Phys. Rev. B **105**, L180409 (2022).